Versatility assessment of supercritical CO2 delamination for photovoltaic modules with EVA, POE or EMAA as encapsulating polymer

Axel Briand, Antoine Leybros, Olivier Doucet, Jean-Christophe Ruiz, Pauline Fontaine-Giraud, Lucas Liotaud, Agnès Grandjean

▶ **To cite this version:**

Axel Briand, Antoine Leybros, Olivier Doucet, Jean-Christophe Ruiz, Pauline Fontaine-Giraud, et al.. Versatility assessment of supercritical CO2 delamination for photovoltaic modules with EVA, POE or EMAA as encapsulating polymer. Journal of Cleaner Production, 2023, 410, pp.137292. 10.1016/j.jclepro.2023.137292 . hal-04702095

HAL Id: hal-04702095
https://hal.science/hal-04702095v1

Submitted on 29 Oct 2024

HAL is a multi-disciplinary open access archive for the deposit and dissemination of scientific research documents, whether they are published or not. The documents may come from teaching and research institutions in France or abroad, or from public or private research centers.

L'archive ouverte pluridisciplinaire **HAL**, est destinée au dépôt et à la diffusion de documents scientifiques de niveau recherche, publiés ou non, émanant des établissements d'enseignement et de recherche français ou étrangers, des laboratoires publics ou privés.

Versatility assessment of supercritical CO_2 delamination for photovoltaic modules with ethylene-vinyl acetate, polyolefin or ethylene methacrylic acid ionomer as encapsulating polymer

Axel Briand[1,2], *Antoine Leybros[1], Olivier Doucet[2], Jean-Christophe Ruiz[1], Pauline Fontaine-Giraud[1], Lucas Liotaud[1], Agnès Grandjean[1]

1- CEA, DES, ISEC, DMRC, Univ Montpellier, Marcoule, France

2- Univ Grenoble Alpes, CEA, DRT, LITEN, DTS, INES, F-38 000 Grenoble, France.

*Corresponding author:

Antoine LEYBROS
CEA
Laboratoire des Procédés Supercritiques et de Décontamination
F-30207 Bagnols sur Cèze
Tel: +33 4 66 79 16 41
Fax: +33 4 66 79 16 41
antoine.leybros@cea.fr

Abstract

The volume of end-of-life photovoltaic panels to be managed will increase considerably over the next decade. In the context of an environmentally friendly circular economy, it is becoming more than necessary to develop efficient recycling processes. In this context, a delamination process using supercritical CO_2 was studied for the recycling of end-of-life photovoltaic modules. The process studied in this work consists of a CO_2 absorption phase within the encapsulating polymer at a pressure level followed by a rapid depressurization leading to the foaming of the polymer. This foaming phenomenon leads to a loss of adhesion at the interfaces of the foamed polymer. Using a systematic experimental protocol, the minimum effective CO_2 temperature and pressure are determined for three various encapsulating polymers: an ethylene-vinyl acetate, a polyolefin and an ethylene methacrylic acid ionomer. Based on this parametric optimization, the levels of separation induced by SC-CO_2 foaming at the interfaces of these

encapsulating polymers in photovoltaic modules are compared. SC-CO_2 treatment therefore seems promising for the delamination of first generation photovoltaic modules and future generations of high efficiency perovskite-based photovoltaic modules containing ionomers. However, the results for the polyolefin indicate that SC-CO_2 treatment is less effective when the encapsulating polymers do not containing CO_2-philic groups.

Keywords: supercritical CO_2, photovoltaic, recycling, polymer, separation

1. Introduction

Photovoltaic (PV) panels are an important component of the ongoing drive toward decarbonised energy generation. Energy production from PV panels has been increasing steadily since the early 2000s and is expected to reach 8,519 GW worldwide in 2050 [1]. However, PV panels only have a lifespan of between 25 and 30 years [2] and the mass of end-of-life panels worldwide is expected to reach between 2 and 8 million tonnes by 2030 [2], with currently no viable outlet.

Crystalline silicon-based PV panels account for almost 95% of the global market [3]. As of 2019, more than 90% had the same multilayer structure (Fig. 1) [3], with a glass plate on the front side, a multilayer polymer backsheet and a crystalline silicon-based cell encapsulated in an elastomer, typically ethylene-vinyl acetate (EVA). These modules are then stiffened by an aluminium frame and electrically connected to a junction box in PV panels. Alternatives for the encapsulating polymer have begun to emerge however. While EVA is still by far the most used (90% of the world market in 2019) [3], the popularity of elastomeric polyolefins (POEs) is increasing (just under 10% of market share in 2019) [3], and while ionomers are yet to be used in mass-produced PV modules, they are considered the best option for next-generation high-efficiency perovskite cells, which are highly sensitive to humidity [4].

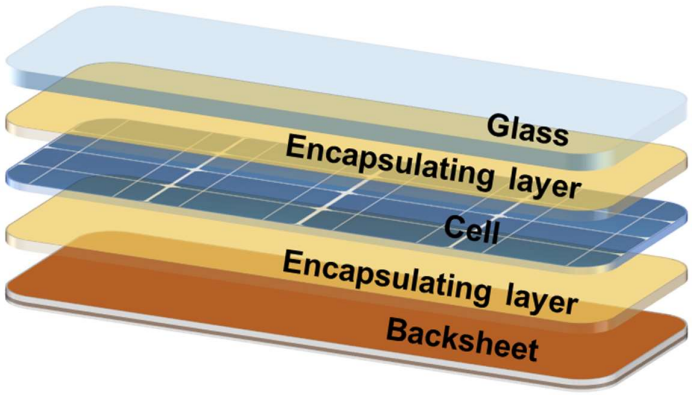

Fig. 1. Schematic representation of the multilayer structure of a photovoltaic module

Recovering metals from spent PV cells is a major economic and environmental challenge. In panels produced before 2014, which are now reaching the end of their lives, silver represents about half (47%) the value per unit mass [2], and even for newer cells, the PV industry is expected to consume almost 70 % of the world's silver production by 2050 [5]. Meanwhile, silicon purification accounts for between 30 and 45 % of the total energy cost of producing a panel [6]. Separating the different layers of the module after removing the panel frame to facilitate recycling therefore makes both ecological and economic sense. Separation processes often involve combinations of mechanical [7,8], thermal [9–11] and/or chemical [12–15] processes. The latter, widely described in the literature [7,8,16], are typically energy-intensive (heat treatments), produce toxic effluents (liquid for chemical treatments, gaseous for heat treatments), or are poorly selective (mechanical treatments). Therefore, the PHOTORAMA project (PHOtovoltaic waste management – advanced Technologies of recovery & recycling of secondary RAw MAterials from end-of-life modules) aims to find new pathways for PV recycling, in a circular economy, using eco-friendly and innovative technologies in all the steps of the global process, in particular for the separation step. The objective of this project is to build a pilot line with a 1000 tons per year capacity, where two separation processes for crystalline silicon-based PV panels are investigated: the cutting of the module with diamond

wire and the delamination using supercritical CO_2. This paper is focused on the supercritical CO_2 delamination process.

Developing an eco-friendly separation process is one of the greatest challenges in recycling PV panels. Supercritical CO_2 (SC-CO_2) is an attractive prospect in this context because CO_2 is a chemically non-contaminating, green solvent [17]. SC-CO_2 treatment is also a dry process with minimal effluent generation that can be operated in closed circuit by recycling the CO_2.

The use of SC-CO_2 with co-solvents has already been described in the literature for the delamination of PV modules [18,19] and other multilayer technological waste such as electronic cards [20,21]. The underlying principle is the same as in chemical delamination however, since it is the co-solvents that dissolve and swell the polymers in the multilayer structure and SC-CO_2 only acts as a carrier fluid to improve the diffusivity of the mixture and reduce the processing time.

In contrast, SC-CO_2 delamination process without co-solvent (Fig. 2a), as developed recently in our laboratory [22,23] exploits CO_2's foaming effect on polymers (Fig. 2b). The resulting mechanical stresses at the interfaces help separate the different layers of the PV module (Fig. 2c), allowing the different components to be recovered and recycled separately.

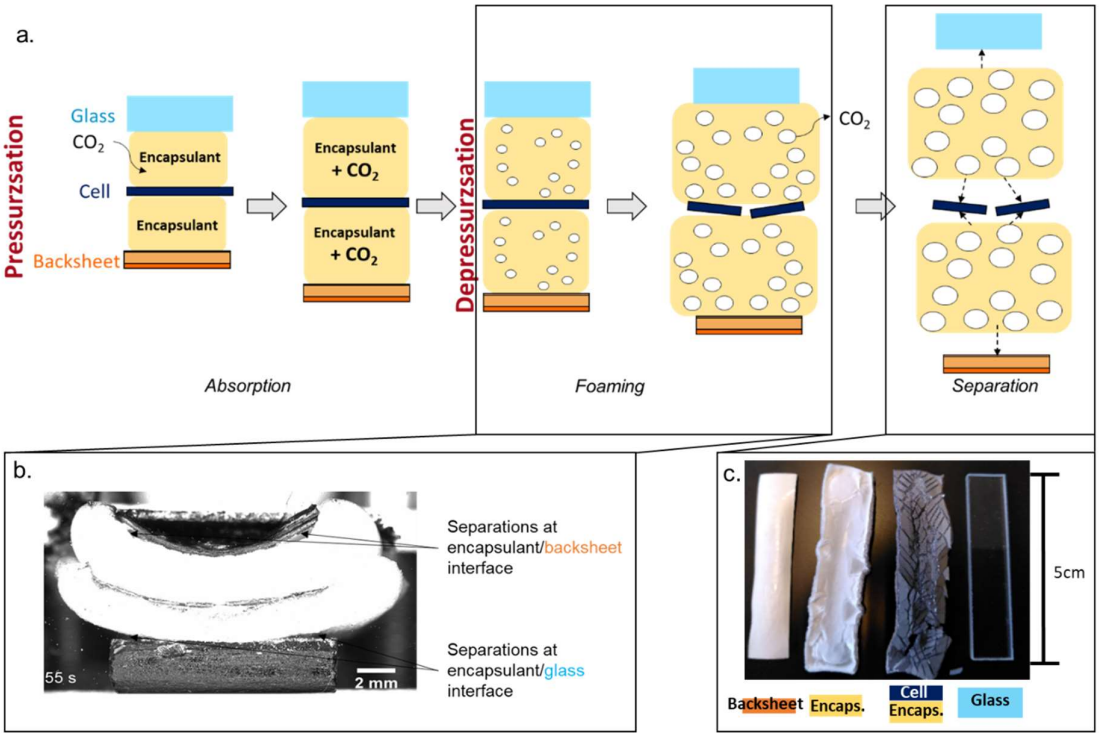

Fig. 2. (a) Schematic representation of the different stages in the supercritical CO_2 delamination process. (b) Deformation-induced separation at photovoltaic module interfaces during depressurization. (c) Photograph of separated photovoltaic module layers after supercritical CO_2 delamination.

The aim of this study was to assess the efficiency of SC-CO_2 delamination for encapsulating polymers other than EVA, in this case a POE and the ionomer ethylene methacrylic acid (EMAA), to strengthen the performance of this process on the PHOTORAMA pilot line. Based on our previous work on EVA, the versatility of the process was evaluated by measuring the level of absorption of the CO_2 into the encapsulating polymer [22] and the foaming window for the encapsulating polymer [23] as a function of its energy cost in terms of temperature, pressure and duration. The solubility and diffusivity of the CO_2 in the encapsulating layer and foaming parameters were measured with a custom-made high-pressure optical device. This methodology would allow to propose guidelines for both recycling and ecological design of non-EVA PV modules. A series of recommendations are proposed to optimize both the recycling and the ecological design of non-EVA PV modules.

2. Material and methods

2.1. Study methodology

Several sets of samples were prepared as detailed below (section 2.2). The minimum treatment temperature was determined by measuring the melting temperature of each encapsulating polymer in CO_2 (section 2.3). The absorption of CO_2 in the encapsulating polymer was evaluated in terms of the solubility and the diffusion coefficient of CO_2 (section 2.4.1). Solubility is a good measure of the affinity of CO_2 for the considered polymers and the diffusion coefficient determines the contact time required to treat the PV modules in CO_2. The minimum pressure was determined by measuring the threshold below which no bubbles form within the encapsulating polymer (section §2.4.2). Together with the melting temperature, this pressure was used to define the foaming window of each encapsulating polymer. Finally, the adhesion losses induced at the encapsulating polymer/glass and encapsulating polymer/backsheet interfaces were measured (section 2.5) to evaluate the efficacy of the process for the considered polymers.

2.2. Materials

The encapsulating polymers used in this study were EVA-28 (Fig. 3a; 600 µm thick; Guangzhou Lushan New Materials Co; Guangdong Province, China), an elastomeric POE (Fig. 3b; 600 µm thick; Mitsui Solar ASCE) and an EMAA ionomer (Fig. 3c; 500 µm thick; Kunran Seal PV 8729D). These three elastomers are rubbery at room temperature (T > glass transition temperature), and cross-linked with peroxide-type units for EVA and the POE and ionic units for EMAA.

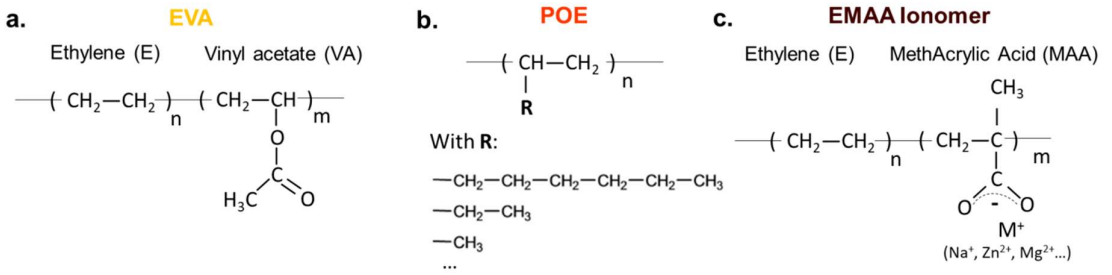

Fig. 3. Chemical structures of the studied encapsulating polymers: (a) ethylene-vinyl acetate, (b) a polyolefin and (c) ethylene methacrylic acid.

The polymers were shaped into thick films for hot lamination (> 120 °C) and used in Si-Al-BSF cells with a 3 mm thick soda-lime glass layer and a primer layer/PET/PVDF backsheet. The different samples used in the study are listed in Table 1.

Table 1. Assemblies used to measure the specified parameters in the encapsulating polymers.

Sample	Description	Size	Structure	Parameters
S1	Laminated encapsulating polymer sheets	5 × 1 cm^2	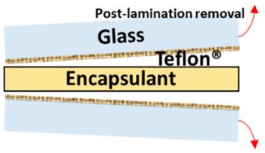	Melting temperature CO_2 solubility CO_2 diffusivity
S2	Backsheet-encapsulated sample	5 × 1 cm^2	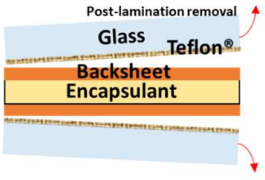	Threshold pressure Bubble radius
S3	Peeling sample	12 × 12 cm^2	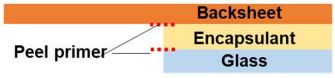	Adhesion loss

2.3. *Melting temperature as a function of CO_2 pressure*

The melting temperatures of the studied encapsulating polymers were measured in CO_2 as a function of pressure by a high pressure differential scanning calorimetry (DSC) (Sensys Evo, Setaram®), using the same protocol as described previously [22].

2.4. *In situ optical observations*

The behaviour of the encapsulating polymers at the different stages of the SC-CO_2 delamination process was observed using an experimental high-pressure device coupled with an optical setup described in detail elsewhere [22,23].

2.4.1. *Study of CO_2 absorption in the encapsulating polymer*

Swelling experiments were performed on S1 samples (Table 1), at 150 bar and temperatures close to the respective melting temperatures of the encapsulating polymers. The level of swelling at equilibrium depends on the solubility of CO_2 in the encapsulating polymer ($\emptyset_1$, in cm^3 of CO_2 per cm^3 of encapsulating polymer) while the swelling kinetics depend on the diffusion coefficient of CO_2 in the polymer (D, in $m^2 \cdot s^{-1}$).

The change in polymer volume was measured as a function of the CO_2 pressure at fixed temperature. In this context, the swelling percentage can be expressed in terms of the volume fraction $\emptyset_1$ as follows [22],

$$\text{Swelling (\%)} = \frac{V_\infty - V_0}{V_0} \times 100 = \frac{\emptyset_1}{1 - \emptyset_1} \times 100 \quad (1)$$

where V_0 and V_∞ are the polymer volumes at the start of the experiment and at equilibrium, respectively. The experimental swelling data were used to adjust the Sanchez-Lacombe equation of state [24,25], yielding the solubility of CO_2 in the polymers as described previously [22].

CO_2 diffusion coefficients in the polymers (D) were obtained from the measured volume changes [26] using the solution of the Fick equation for diffusion across a sheet [27]:

$$\frac{V_t - V_0}{V_\infty - V_0} = 1 - \sum_{n=0}^{\infty} \frac{8}{(2n+1)^2 \pi^2} exp(-D(2n+1)^2 \pi^2 t / 4l^2) \quad (2)$$

where V_t is the polymer volume at time t (s) and l (m) is the thickness of the sample.

2.4.2. Polymer foaming measurements

The threshold foaming pressure at a given temperature was defined as the lowest pressure at which microscopic bubbles formed in the polymers during depressurisation. In-situ bubble observations were performed on S2 samples (Table 1), at temperatures close to the respective melting temperatures of the polymers. A backsheet/encapsulating polymer/backsheet arrangement was chosen instead of the backsheet/polymer/glass structure of actual PV modules because the glass layer scatters and reflects light, which would have degraded the quality of the images obtained. The extra backsheet was added as a barrier to limit CO_2 diffusion during depressurisation (just as the glass layer would in a standard PV module).

The images of the bubbles (Fig. 4a) were binarized (Fig. 4b), segmented and labelled using Image J® , to measure the size of their projected areas (Fig. 4c).

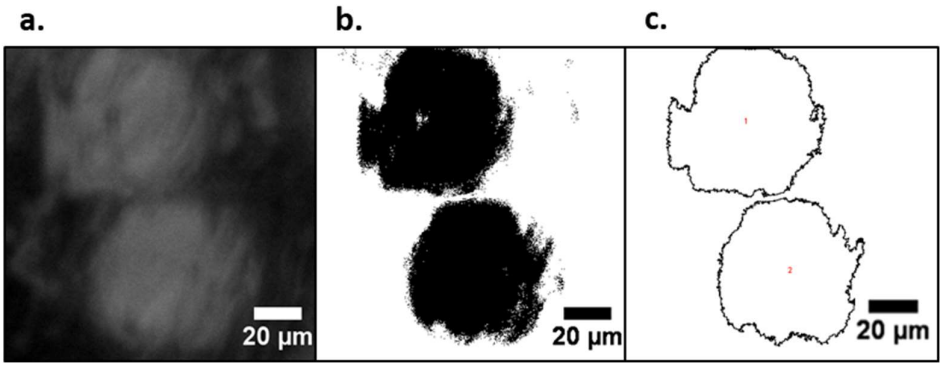

Fig. 4. Illustration of the image processing steps performed with Image J® on two bubbles: (a) raw image, (b) the same image after binarization and (c) the extracted bubble contours.

Modelling the bubbles as spherical, the measured projected areas were converted to two-dimensional equivalent radii (µm) using the standard formula:

$$\text{Radius } (\mu m) = \sqrt{\frac{\text{Projected bubble surface area } (\mu m^2)}{\pi}} \quad \textbf{(3)}$$

The bubble density was then calculated using**:**

$$\text{Bubble density } (m^{-3}) = \frac{\text{Number of bubbles detected}}{\text{Volume of encapsulating polymer } (m^3)} \quad \textbf{(4)}$$

where the volume of encapsulating polymer was estimated as the product of the observed area and the focal depth (0.2 mm with this experimental setup). Characteristic bubble sizes were measured at the time of maximum bubble density (see Supplementary Material), corresponding to the end of the nucleation phase.

2.5. Delamination experiments

Adhesion loss at the different interfaces of a PV module was measured as described previously [23] after treating the samples (S3, Table 1) in SC-CO_2 for 6 hours at the lowest possible temperature (the melting temperature of the respective polymers) and pressure (150 bar, to ensure bubble nucleation in all three polymers).

The SC-CO_2 treatments were performed in a pilot reactor (Matcos 4&5, Separex®; internal diameter, 190 mm) equipped with a 12 L autoclave (Fig. 5). The samples were positioned vertically in the reactor. The highest possible depressurisation rate was used (2.7 bar·s^{-1}) to maximize the mechanical stress induced by the foaming of the encapsulating polymers [23]. The system was controlled and the operating parameters were adjusted using computer software.

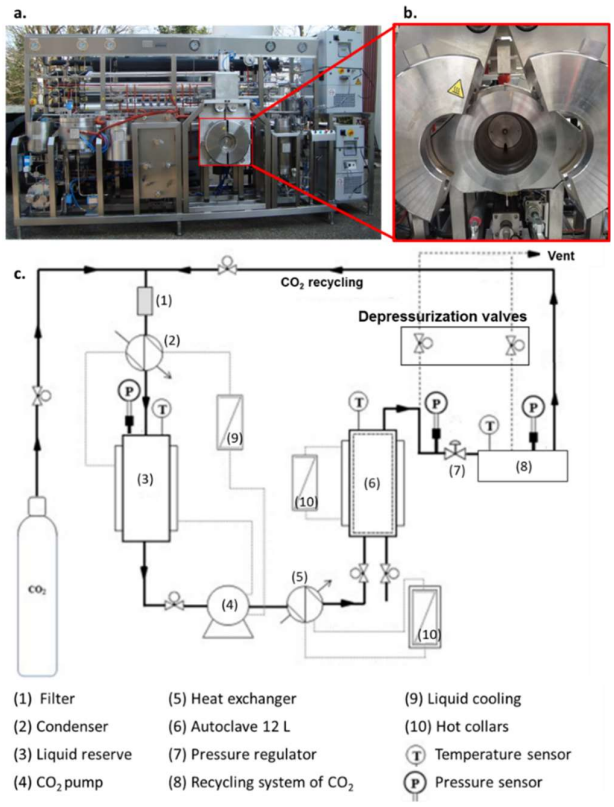

Fig. 5. (a, b) Photographs of (a) the pilot reactor and (b) the autoclave and (c) flow diagram of the system.

The adhesion strength of the surfaces in contact with the encapsulating polymer layers was measured before after SC-CO_2 treatment using 180° peel tests, performed on a universal testing machine (S6800, Instron®). The loss of adhesion due to the SC-CO_2 treatment was calculated from the measured values using Eq. (5),

$$\text{Adhesion loss (\%)} = \frac{\overline{PS_{REF}} - \overline{PS_{CO2}}}{\overline{PS_{REF}}} \times 100 \quad \textbf{(5)}$$

where $\overline{PS_{REF}}$ is the reference peel strength measured before treatment and $\overline{PS_{CO2}}$ is the peel strength measured after SC-sCO_2 treatment.

3. Results and discussion

3.1. Melting temperatures

Below the melting temperature, the crystallites in the polymer act as nodes that limit expansion during foaming. Increasing the processing temperature to near or above the melting temperature lowers the stiffness of the polymer [28–30] and promotes expansion during foaming [23,31], which maximizes the mechanical stress at the different interfaces and therefore the level of delamination obtained. The melting temperature is therefore the minimum temperature for effective SC-CO_2 delamination. Measurements were performed at different pressures because melting temperatures in CO_2 can vary with pressure [32,33].

The melting temperatures of EMAA, EVA and the POE in CO_2 are 90, 75 and 60°C, respectively. Fig. 6 shows that these values vary little with pressure, decreasing by just 2 to 6°C between 0 and 150 bar. Note that measurements for the POE could not be performed above 73.8 bar because the melting peak of this polymer is too close to the critical point, which prevents the measurement of a sufficient reference baseline [33].

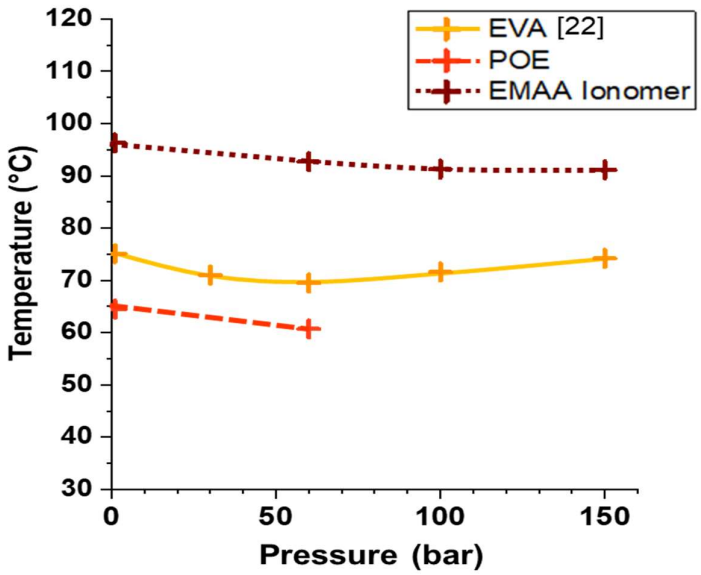

Fig. 6. Melting temperatures of the studied polymers (ethylene-vinyl acetate (EVA), a polyolefin (POE) and ethylene methacrylic acid (EMAA)) as a function of CO_2 pressure. Lines are added to guide the eye.

Subsequent experiments were therefore performed at 60°C for the POE, 75°C for EVA and 90°C for EMAA.

3.2. CO_2 absorption into the encapsulating polymer

3.2.1. CO_2 solubility

The swelling curves obtained for the POE and EMAA are compared with those measured previously for EVA [22] in Fig. 7.

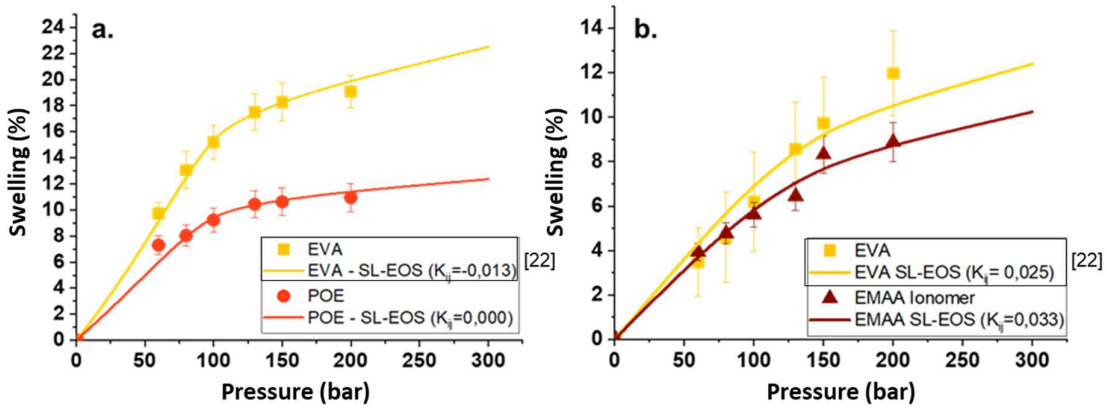

Fig. 7. Experimental swelling curves (points) and fits with the Sanchez-Lacombe equation of state (lines) for (a) ethylene-vinyl acetate (EVA) and a polyolefin (POE) at 60°C and (b) EVA and ethylene methacrylic acid (EMAA) at 90°C.

The parameters used to fit the data with the Sanchez-Lacombe equation of state are shown in

Table 2 [22] [34] [35]. The experimental data are well modelled by this equation, with a relative deviation of just 5.1% for POE and 4.5% for EMAA.

Table 2. Parameters of the Sanchez-Lacombe equation of state for CO_2 and the different polymers studied

Parameters	CO_2	EVA	POE[a]	EMAA[b]
M_i ($kg \cdot mol^{-1}$)	0.044	35	90	76
T_i* (K)	300	635	665	662
P_i* (MPa)	650	460	341	499
ρ_i* ($kg \cdot m^{-3}$)	1515	945	880	950
K_{ij} (AARD %)	60 °C	−0.013 (2.9 %)	0.000 (5.1 %)	
	75 °C	0.007 (5.5 %)		
	90 °C	0.025 (11.1 %)		0.033 (4.5 %)

EVA, ethylene-vinyl acetate; POE, polyolefin; EMAA, ethylene methacrylic acid; K_{ij}, binary interaction coefficient; AARD, average absolute relative deviation

[a]based on values for high-density polyethylene [35]

[b]based on values for ethylene ethyl acrylate [35]

The binary interaction coefficient (Kij) reflects how much the system deviates from ideal behaviour and provides information on the chemical affinity between CO_2 and the studied polymers, with lower values indicating greater affinity [36]. This parameter varies with temperature [37] so the measurements with EVA were repeated at the melting temperatures of the POE and of EMAA. The lower values obtained (Table 2) show that EVA has a greater affinity for CO_2 than do the two other polymers.

The volume fraction of CO_2 in the three polymers as a function of pressure (Fig. 8) was obtained from the fits to the Sanchez-Lacombe equation of state.

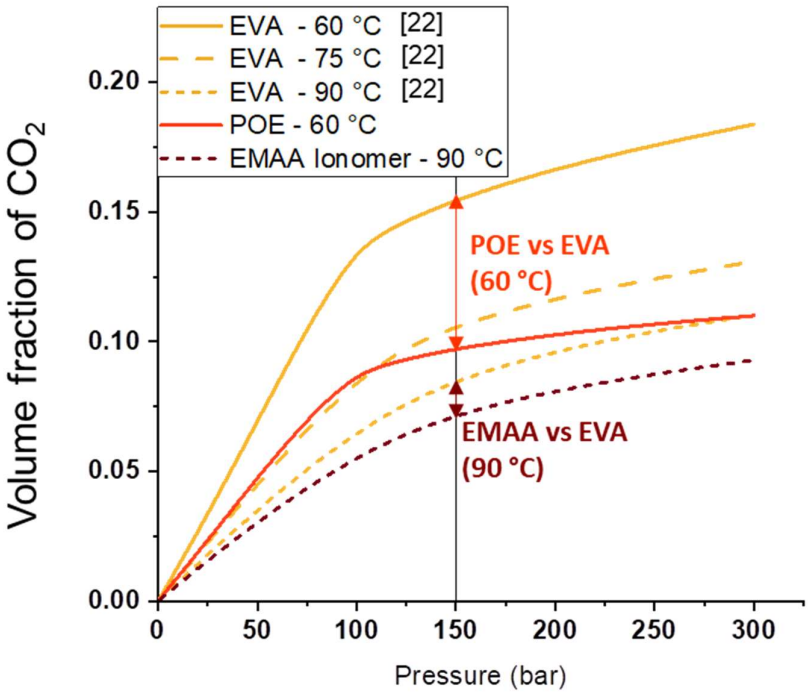

Fig. 8. Volume fraction of CO_2 in the studied polymers (ethylene-vinyl acetate (EVA), a polyolefin (POE) and ethylene methacrylic acid (EMAA)) as a function of CO_2 pressure.

In keeping with the values obtained for K_{ij} (Table 2), Fig. 8 shows that at 60°C, CO_2 is nearly two times less soluble in the POE than in EVA, but is only slightly less soluble in EMAA than in EVA at 90 °C. These results also show that the solubility of CO_2 in the different polymers increases only increases slightly above 130 bar.

The lower solubility of CO_2 in the POE, and to a lesser extent in EMAA, than in EVA, can be explained by the absence of carbonyl groups in the former (Fig. 3). Indeed, the strong Lewis acid-Lewis base interactions between the carbon atom in CO_2 and the carbonyl oxygen [38,39] promotes the absorption of CO_2 into EVA. In contrast, the Lewis acid-Lewis base interactions between the hydrogen atoms of the ethylene units and the oxygen of CO_2 are much weaker [39]. For EMAA, the carboxylate group appears to play the same role as carbonyl in increasing the polymer's affinity for CO_2. However, these groups are less accessible than carbonyls because

the ionic interactions in EMAA lead to the creation of dense zones that limit the penetration of SC-CO_2 [40].

3.2.2. CO_2 diffusivity

Fig. 9 highlights the difference in swelling kinetics between the studied polymers. The experimental curves were fitted using the Fick diffusion equation (Eq. 2) to obtain the CO_2 diffusion coefficients in the studied polymers [22]. The diffusivity of CO_2 is about three times lower in the POE and thirteen times lower in EMAA than in EVA. These differences are consistent with the differences in CO_2/polymer affinities discussed above. These much lower diffusion constants may be a limiting factor for SC-CO_2 delamination of PV modules composed of POEs or EMAA, because they imply much longer treatment times.

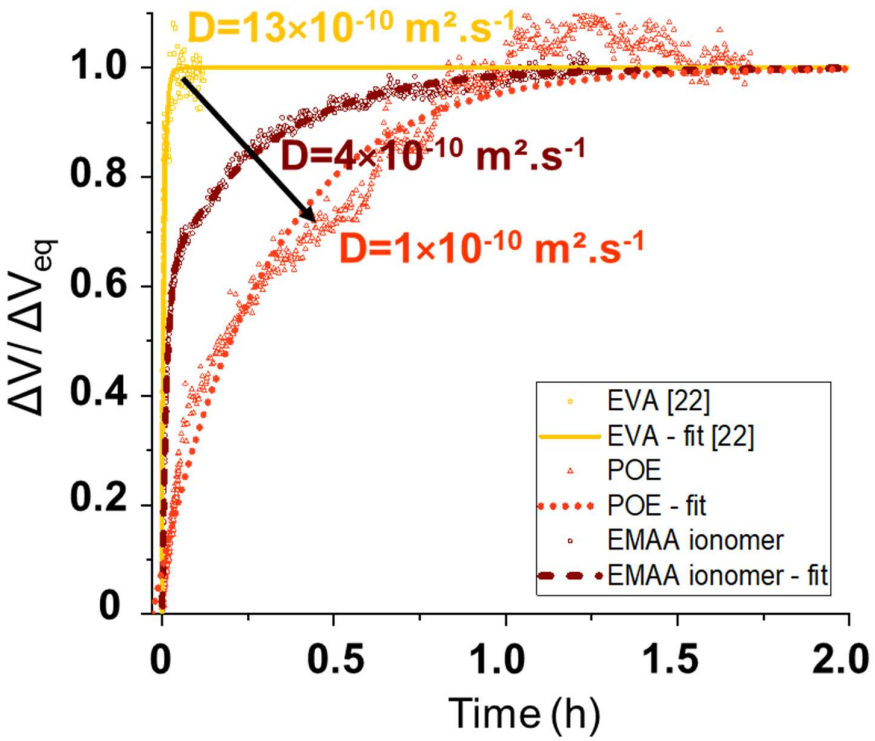

Fig. 9. Swelling kinetics of the studied polymers (ethylene-vinyl acetate (EVA), a polyolefin (POE) and ethylene methacrylic acid (EMAA)) measured at 150 bar and temperatures close to

the melting point (60°C for POE, 75°C for EVA and 90°C for the EMAA). The solid lines are fits to the Fick diffusion equation (Eq. 2) and the corresponding CO_2 diffusion coefficients (D) are shown alongside.

3.3. Threshold foaming pressure

Fig. 10 shows images of the bubbles formed in the three polymers at a pressure of 150 bar and a depressurisation rate of 1.7 bar·s^{-1}. The clear differences in the size and density of the bubbles illustrate the distinct behaviours of each of the polymers in SC-CO_2.

.

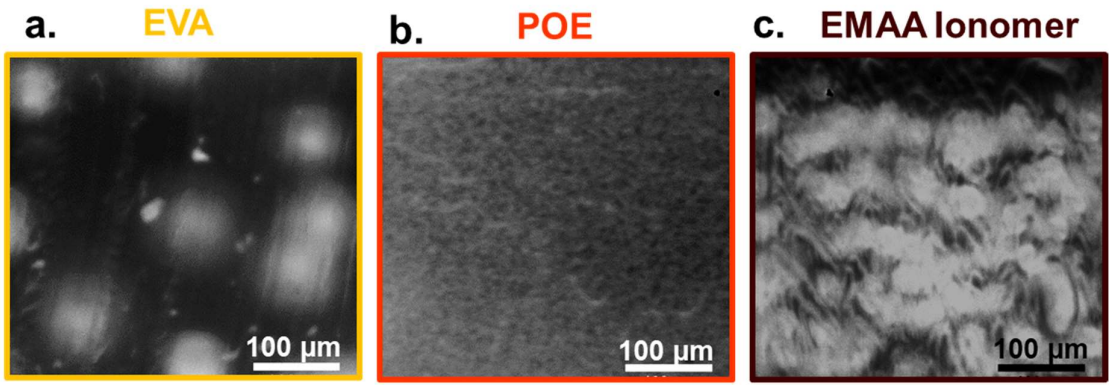

Fig. 10. Optical micrographs of the bubbles formed at 150 bar and 1.7 bar·s^{-1} in (a) EVA at 75°C, (b) the POE at 60°C and (c) EMAA at 90°C.

The average radii of the bubbles ($\overline{R_{eq}}$ in m) are plotted as a function of the bubble density (d_{bubble} in m^{-3}) in Fig. 11 for the three polymers These curves were fitted using an empirical relationship (Eq. 6), which is independent of the operating parameters:

$$\overline{R_{eq}}\left(\overline{\sqrt[3]{d_{bubble}}}\right) = A_1\, exp\left(-\frac{\overline{\sqrt[3]{d_{bubble}}}}{b_1}\right) + A_2 exp\left(-\frac{\overline{\sqrt[3]{d_{bubble}}}}{b_2}\right) + \overline{R_{min}} \qquad \textbf{(6)}$$

These fits were used to calculate the average minimum equivalent radius ($\overline{R_{min}}$) of the bubbles in each polymer, 0.2 µm in the POE, 1.5 µm in EMAA and 4.2 µm in EVA. This information is important for delamination applications, because previous results suggest that to achieve layer separation, the bubbles formed must be smaller than the microstructural features of the adhering material [23].

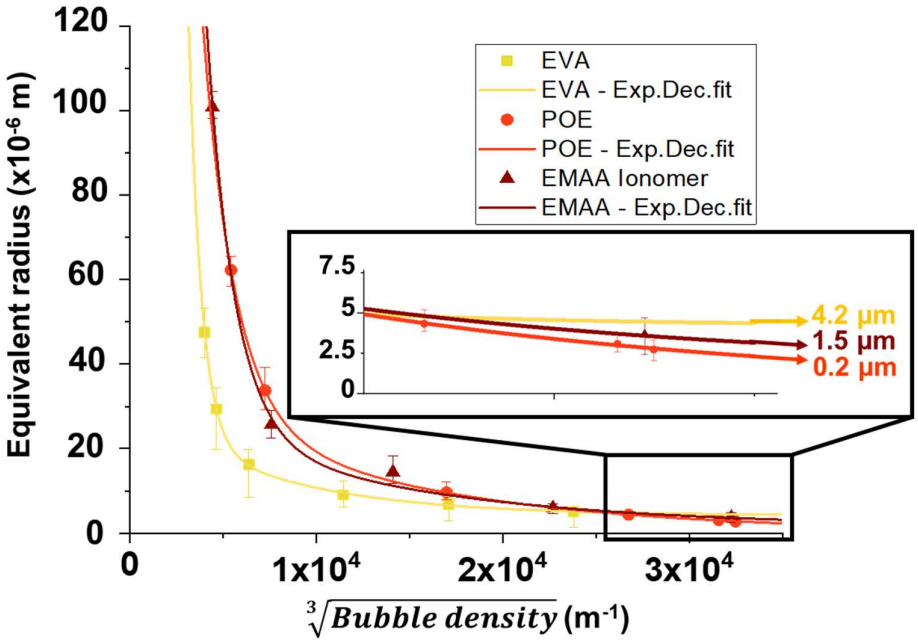

Fig. 11. Average equivalent bubble radius as a function of the cube root of the bubble density measured for the studied polymers close to the melting temperature at pressures of 100–200 bar and depressurization rates of 1.0–2.7 bar·s^{-1}. The solid lines are fits using Eq. (6).

Fig. 12 shows how the size of the first bubbles formed evolves as a function of pressure in the studied polymers. The experimental data were fitted to a negative exponential function similar to the classical nucleation relationship between bubble density and pressure applied to polymer foaming in SC-CO_2 [41–43]. Here, these curves help identify the threshold pressure below which no bubbles are formed by homogeneous nucleation in the three polymers: roughly

100 bar for the POE, 120 bar for EMAA and about 140 bar for EVA. These are the lowest pressures at which SC-CO_2 delamination processes should be performed for these polymers.

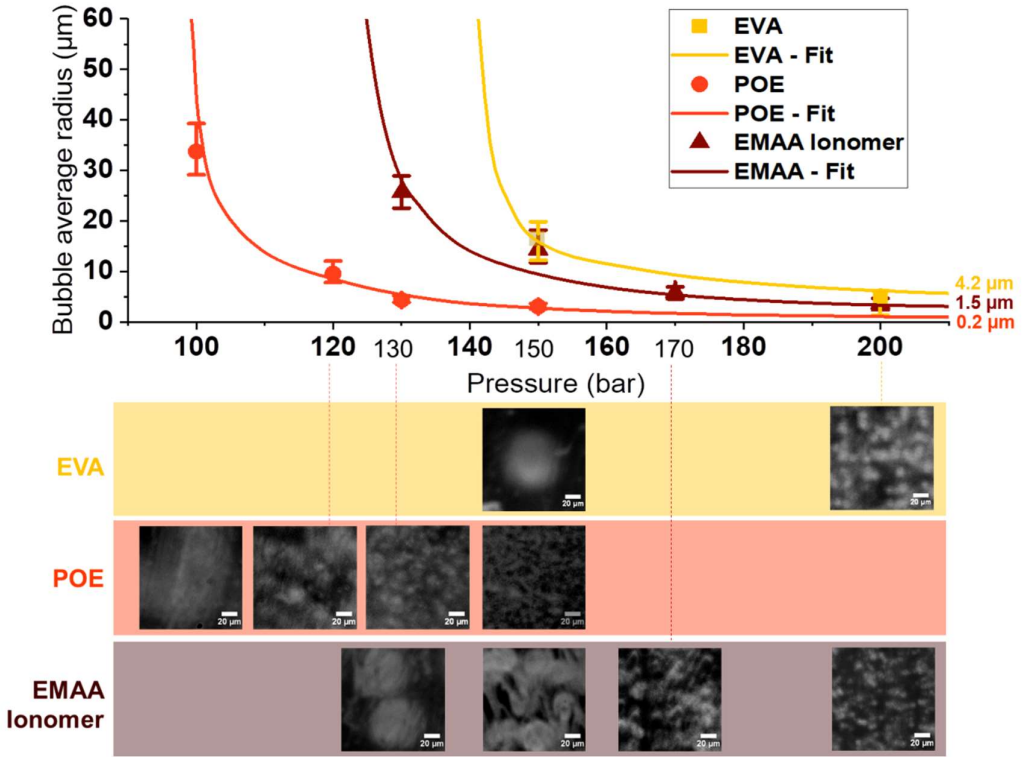

Fig. 12. Average radius of the first bubbles formed as a function of pressure at a fixed temperature (close to the melting point of the polymers) and depressurisation rate (1.7 bar·s^{-1}) in ethylene-vinyl acetate (EVA), a polyolefin (POE) and ethylene methacrylic acid (EMAA). The solid lines are fits to a negative exponential function [41–43].

3.4. Separation at photovoltaic module interfaces

Fig. 13 compares the adhesion loss at the two interfaces of each polymer after SC-CO_2 treatment at the lowest possible temperature. At the polymer/backsheet interface, the adhesion loss was greater than 80% in each case, probably because the backsheet primer layer is made

with EVA and is affected in a similar way by the SC-CO_2 treatment for all three encapsulating polymers. This result is important because the presence of fluorinated polymers in backsheets is the main limitation for the use of thermal processes in PV module recycling, to avoid the release of highly toxic gases (fluorocarbon, hydrofluoric acid...) [9]. However, removing the backsheet thanks to a brief SC-CO_2 treatment would allow the remaining, partially attached encapsulating polymer to be removed effectively from the cell by subsequent thermal treatment (Fig. 2c).

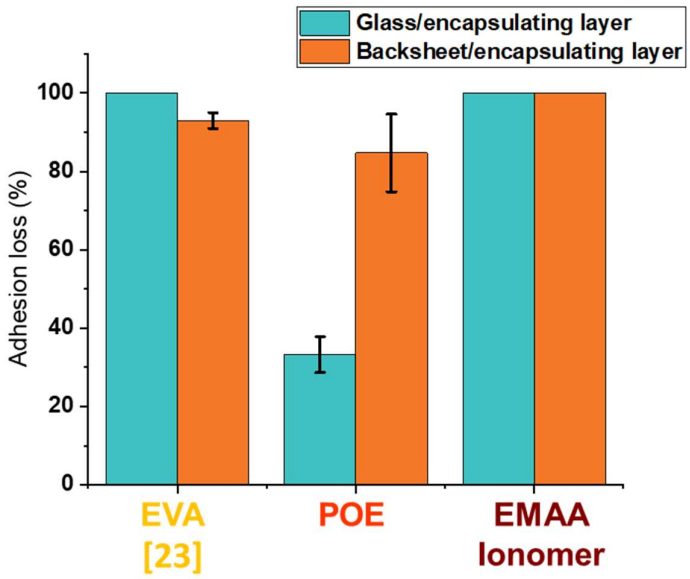

Fig. 13. Adhesion loss (%) at the encapsulating layer/glass and encapsulating layer/backsheet interfaces of ethylene-vinyl acetate (EVA), the polyolefin (POE) and ethylene methacrylic acid (EMAA) at the respective melting temperatures (60°C for POE, 75°C for EVA and 90°C for the EMAA), a pressure of 150 bar, a depressurization rate of 2.7 bar·s^{-1}, and a treatment time of 6 h.

The separated interfaces were characterized by Raman spectroscopy to identify the delamination type that occurred by looking for the spectral signatures of encapsulating layers

(see supplementary material) on separated materials (glass or backsheet). All separations were interfacial. At the polymer/glass interface, complete separation was obtained for EVA and EMAA (Fig. 13). The loss of adhesion was much lower at the POE/glass interface, in keeping with the lower affinity and solubility of CO_2 in the POE, which limit the expansion of the polymer and the induced mechanical stress during depressurization. This result highlights the importance of considering the chemical structure of the encapsulating polymer before performing SC-CO_2 delamination. One possibility to improve separation at POE/glass interfaces may be to increase the temperature of the treatment, to increase the flexibility of the polymer and promote expansion [23].

4. Conclusion

The performance of SC-CO_2 treatment for the delamination of PV modules with EVA, a POE or EMAA encapsulating layers was characterized using a well-defined study methodology. The minimal treatment temperature for each polymer was determined by measuring the respective melting temperatures: approximately 60°C for the POE, 75°C for EVA and 90°C for EMAA. The treatment times required for each polymer were estimated from the CO_2 diffusion coefficients in the polymers, 13×10^{-10} $m^2 \cdot s^{-1}$ for EVA, 4×10^{-10} $m^2 \cdot s^{-1}$ for EMAA, and 1×10^{-10} $m^2 \cdot s^{-1}$ for the POE, obtained by fitting experimental swelling kinetics curves. Finally, the minimal treatment pressure for each polymer was deduced from measurements of the threshold pressure for bubble nucleation, which was estimated at 100 bar for the POE, 120 bar for EMAA and about 140 bar for EVA.

Separation experiments on PV module interfaces showed that the efficiency of the SC-CO_2 process depends on the affinity of CO_2 for the encapsulating polymer, which was high for EVA, intermediate for EMAA, and relatively low for the POE. SC-CO_2 treatment therefore seems promising for the delamination of first generation EVA-based PV modules and future

generations of high efficiency perovskite-based photovoltaic modules containing ionomers such as EMAA. However, the results for the POE indicate that SC-CO_2 treatment is less effective when the encapsulating polymers do not containing CO_2-philic groups. A limitation of SC-CO_2 delamination for PV modules is therefore that its efficiency depends on the chemical structure of the encapsulating polymer(s). Conversely, this limitation could be taken into account in the design of PV panels and other sources of electronic waste to facilitate end-of-life recycling, which is often hindered by a lack of standardization.

Acknowledgements

This project has received funding from the European Union's Horizon2020 Program for research, technological development and demonstration under Grant Agreement N° 958223.

References

[1] IRENA, Future of solar photovoltaic : Deployment, investment, technology, grid integration and socio-economic aspects, International Renewable Energy Agency, 2019.
[2] I. IRENA, End-Of-Life Management: Solar Photovoltaic Panels, Int. Renew. Energy Agency Int. Energy Agency Photovolt. Power Syst. (2016).
[3] ITRPV, International Technology Roadmap for Photovoltaic (ITRPV) - Results of 2019 - 11th edition, 2020.
[4] J. Tracy, N. Bosco, C. Delgado, R. Dauskardt, Durability of ionomer encapsulants in photovoltaic modules, Sol. Energy Mater. Sol. Cells. 208 (2020). https://doi.org/10.1016/j.solmat.2020.110397.
[5] S. Lo Piano, J. Sluijs, A. Saltelli, Silver as a Constraint for a Large-Scale Development of Solar Photovoltaics? Scenario-Making to the Year 2050 Supported by Expert Engagement and Global Sensitivity Analysis, Front. Energy Res. 7 (2019). https://doi.org/10.3389/fenrg.2019.00056.
[6] J.H. Wong, M. Royapoor, C.W. Chan, Review of life cycle analyses and embodied energy requirements of single-crystalline and multi-crystalline silicon photovoltaic systems, Renew. Sustain. Energy Rev. 58 (2016) 608–618. https://doi.org/10.1016/j.rser.2015.12.241.
[7] V. Savvilotidou, E. Gidarakos, Pre-concentration and recovery of silver and indium from crystalline silicon and copper indium selenide photovoltaic panels, J. Clean. Prod. 250 (2020). https://doi.org/10.1016/j.jclepro.2019.119440.
[8] R. Deng, Y. Zhuo, Y. Shen, Recent progress in silicon photovoltaic module recycling processes, Resour. Conserv. Recycl. 187 (2022) 106612. https://doi.org/10.1016/j.resconrec.2022.106612.

[9] V. Fiandra, L. Sannino, C. Andreozzi, G. Graditi, End-of-life of silicon PV panels: A sustainable materials recovery process, Waste Manag. 84 (2019) 91–101. https://doi.org/10.1016/j.wasman.2018.11.035.
[10] C.E.L. Latunussa, F. Ardente, G.A. Blengini, L. Mancini, Life Cycle Assessment of an innovative recycling process for crystalline silicon photovoltaic panels, Life Cycle Environ. Ecol. Impact Anal. Sol. Technol. 156 (2016) 101–111. https://doi.org/10.1016/j.solmat.2016.03.020.
[11] F. Ardente, C.E.L. Latunussa, G.A. Blengini, Resource efficient recovery of critical and precious metals from waste silicon PV panel recycling, Waste Manag. 91 (2019) 156–167. https://doi.org/10.1016/j.wasman.2019.04.059.
[12] Y. Kim, J. Lee, Dissolution of ethylene vinyl acetate in crystalline silicon PV modules using ultrasonic irradiation and organic solvent, Sol. Energy Mater. Sol. Cells. 98 (2012) 317–322. https://doi.org/10.1016/j.solmat.2011.11.022.
[13] T. Doi, I. Tsuda, H. Unagida, A. Murata, K. Sakuta, K. Kurokawa, Experimental study on PV module recycling with organic solvent method, PVSEC 11 - PART III. 67 (2001) 397–403. https://doi.org/10.1016/S0927-0248(00)00308-1.
[14] P. Dias, L. Schmidt, M. Monteiro Lunardi, N.L. Chang, G. Spier, R. Corkish, H. Veit, Comprehensive recycling of silicon photovoltaic modules incorporating organic solvent delamination – technical, environmental and economic analyses, Resour. Conserv. Recycl. 165 (2021) 105241. https://doi.org/10.1016/j.resconrec.2020.105241.
[15] S. Kang, S. Yoo, J. Lee, B. Boo, H. Ryu, Experimental investigations for recycling of silicon and glass from waste photovoltaic modules, Renew. Energy. 47 (2012) 152–159. https://doi.org/10.1016/j.renene.2012.04.030.
[16] R. Deng, N.L. Chang, Z. Ouyang, C.M. Chong, A techno-economic review of silicon photovoltaic module recycling, Renew. Sustain. Energy Rev. 109 (2019) 532–550. https://doi.org/10.1016/j.rser.2019.04.020.
[17] D. Bégin, C. Couture, M. Gérin, M. Debia, Solvants verts: Fondements, santé, sécurité, environnement et substitution, IRSST, 2020. https://www.irsst.qc.ca/media/documents/PubIRSST/R-1089.pdf.
[18] C. Aymonier, C. Slostowski, Method and device for dismantling multilayer systems including at least one organic component, WO/2017/037260, 2017.
[19] É.S. Lovato, L.M. Donato, P.P. Lopes, E.H. Tanabe, D.A. Bertuol, Application of supercritical CO2for delaminating photovoltaic panels to recover valuable materials, J. CO2 Util. 46 (2021). https://doi.org/10.1016/j.jcou.2021.101477.
[20] S. Sanyal, Q. Ke, Y. Zhang, T. Ngo, J. Carrell, H. Zhang, L.L. Dai, Understanding and optimizing delamination/recycling of printed circuit boards using a supercritical carbon dioxide process, J. Clean. Prod. 41 (2013) 174–178. https://doi.org/10.1016/j.jclepro.2012.10.011.
[21] E. Hsu, C.J. Durning, A.C. West, A.-H.A. Park, Enhanced extraction of copper from electronic waste via induced morphological changes using supercritical CO2, Resour. Conserv. Recycl. 168 (2021) 105296. https://doi.org/10.1016/j.resconrec.2020.105296.
[22] A. Briand, A. Leybros, C. Audoin, J.C. Ruiz, F. Lamadie, A. Grandjean, CO2 absorption into a polymer within a multilayer structure: The case of poly(ethylene-co-vinyl acetate) in photovoltaic modules, J. Supercrit. Fluids. 179 (2022) 105380. https://doi.org/10.1016/j.supflu.2021.105380.
[23] A. Briand, A. Leybros, O. Doucet, M. Vite, A. Gasmi, J.C. Ruiz, F. Lamadie, A. Grandjean, Deformation-induced delamination of photovoltaic modules by foaming ethylene-vinyl acetate with supercritical CO2, J. CO2 Util. 59 (2022) 101933. https://doi.org/10.1016/j.jcou.2022.101933.
[24] I.C. Sanchez, R.H. Lacombe, Statistical Thermodynamics of Polymer Solutions, Macromolecules. 11 (1978) 1145–1156. https://doi.org/10.1021/ma60066a017.

[25] C. Panayiotou, I.C. Sanchez, Swelling of network structures, Polymer. 33 (1992) 5090–5093. https://doi.org/10.1016/0032-3861(92)90064-4.
[26] J.R. Royer, J.M. DeSimone, S.A. Khan, Carbon dioxide-induced swelling of poly(dimethylsiloxane), Macromolecules. 32 (1999) 8965–8973. https://doi.org/10.1021/ma9904518.
[27] J. Crank, The Mathematics of Diffusion, Second Edition, Brunel University Uxbridge, 1975.
[28] S. Curia, D.S.A. De Focatiis, S.M. Howdle, High-pressure rheological analysis of CO2-induced melting point depression and viscosity reduction of poly(ε-caprolactone), Self-Heal. Polym. 69 (2015) 17–24. https://doi.org/10.1016/j.polymer.2015.05.026.
[29] R. Liao, W. Yu, C. Zhou, Rheological control in foaming polymeric materials: II. Semi-crystalline polymers, Polymer. 51 (2010) 6334–6345. https://doi.org/10.1016/j.polymer.2010.11.001.
[30] J.A. Sarver, J.C. Hassler, E. Kiran, Linking thermophysical and rheological properties to the selection of CO2 foaming conditions of rubbery elastomers using the relative rigidity reduction path, J. Supercrit. Fluids. 166 (2020). https://doi.org/10.1016/j.supflu.2020.105015.
[31] E. Reverchon, S. Cardea, Production of controlled polymeric foams by supercritical CO2, J. Supercrit. Fluids. 40 (2007) 144–152. https://doi.org/10.1016/j.supflu.2006.04.013.
[32] Z. Zhong, S. Zheng, Y. Mi, High-pressure DSC study of thermal transitions of a poly(ethylene terephthalate)/carbon dioxide system, Polymer. 40 (1999) 3829–3834. https://doi.org/10.1016/S0032-3861(98)00594-1.
[33] E. Huang, X. Liao, C. Zhao, C.B. Park, Q. Yang, G. Li, Effect of Unexpected CO2's Phase Transition on the High-Pressure Differential Scanning Calorimetry Performance of Various Polymers, ACS Sustain. Chem. Eng. 4 (2016) 1810–1818. https://doi.org/10.1021/acssuschemeng.6b00008.
[34] F. Doghieri, G.C. Sarti, Nonequilibrium Lattice Fluids: A Predictive Model for the Solubility in Glassy Polymers, Macromolecules. 29 (1996) 7885–7896. https://doi.org/10.1021/ma951366c.
[35] S. Areerat, E. Funami, Y. Hayata, D. Nakagawa, M. Ohshima, Measurement and prediction of diffusion coefficients of supercritical CO2 in molten polymers, Polym. Eng. Sci. 44 (2004) 1915–1924. https://doi.org/10.1002/pen.20194.
[36] M.B. Kiszka, M.A. Meilchen, M.A. McHugh, Modeling high-pressure gas–polymer mixtures using the sanchez-lacombe equation of state, J. Appl. Polym. Sci. 36 (1988) 583–597. https://doi.org/10.1002/app.1988.070360311.
[37] Z. Chen, K. Cao, Z. Yao, Z. Huang, Modeling solubilities of subcritical and supercritical fluids in polymers with cubic and non-cubic equations of state, J. Supercrit. Fluids. 49 (2009) 143–153. https://doi.org/10.1016/j.supflu.2008.12.013.
[38] S.G. Kazarian, M.F. Vincent, F.V. Bright, C.L. Liotta, C.A. Eckert, Specific Intermolecular Interaction of Carbon Dioxide with Polymers, J. Am. Chem. Soc. 118 (1996) 1729–1736. https://doi.org/10.1021/ja950416q.
[39] A. Dardin, J.M. DeSimone, E.T. Samulski, Fluorocarbons dissolved in supercritical carbon dioxide. NMR evidence for specific solute-solvent interactions, J. Phys. Chem. B. 102 (1998) 1775–1780. https://doi.org/10.1021/jp972127p.
[40] J.A. Sarver, J.A. Rasco, X. Jiang, J. Van Dun, E. Kiran, Physical Foaming of an Ethylene/Acrylic Acid/n-Butyl Acrylate Ionomer with Carbon Dioxide, Ind. Eng. Chem. Res. 60 (2021) 14213–14224. https://doi.org/10.1021/acs.iecr.1c02337.
[41] S. Siripurapu, J.A. Coughlan, R.J. Spontak, S.A. Khan, Surface-constrained foaming of polymer thin films with supercritical carbon dioxide, Macromolecules. 37 (2004) 9872–9879. https://doi.org/10.1021/ma0484983.

[42] S.K. Goel, E.J. Beckman, Nucleation and growth in microcellular materials: Supercritical CO2 as foaming agent, AIChE J. 41 (1995) 357–367. https://doi.org/10.1002/aic.690410217.
[43] I. Tsivintzelis, G. Sanxaridou, E. Pavlidou, C. Panayiotou, Foaming of polymers with supercritical fluids: A thermodynamic investigation, J. Supercrit. Fluids. 110 (2016) 240–250. https://doi.org/10.1016/j.supflu.2015.11.025.